OPEN ACCESS

ACTA METALLURGICA SLOVACA

2024, VOL. 30, NO. 4, 156-159

RESEARCH PAPER

HEAT TREATMENT EFFECT ON THE INTERMETALLIC Al-Fe-Si ALLOY MICROSTRUCTURE

Violetta Andreyachshenko[1,*], *Gulnara Ulyeva*[2]

[1] Abylkas Saginov Karaganda Technical University, 100027, Karaganda, Kazakhstan, Vi-ta.z@mail.ru,
[2] Qarmet, 101400, Temirtau, Kazakhstan, granatik73@mail.ru

*Corresponding author: Vi-ta.z@mail.ru, tel.: 87013962994, Abylkas Saginov Karaganda Technical University, 100027, Karaganda, Kazakhstan

Received: 05.11.2024
Accepted: 16.11.2024

ABSTRACT

The Al-Fe-Si system has been the focus of attention of world science for a long time, but there are still unknown scientific areas. A system that provides a fully intermetallic phase composition has been considered, which is a very relevant approach and is of particular interest. In this paper, based on modeling, the phase composition of an alloy rich in silicon and iron has been predicted using commercial starting materials. Heat treatment of the alloy has been carried out using two cooling methods: water and air. It has been found that with accelerated cooling in water, the α ↔ β transition is partially suppressed with the formation of a double intermetallic phase θ, with the replacement of some aluminum atoms with silicon atoms. When cooling in air, the dominant phase is the θ phase; the transition θ' with a reduced iron content has been detected.

Keywords: intermetallic phase; heat treatment; multicomponent system; aluminum alloy; solid solution; phase transition

INTRODUCTION

In recent decades, multicomponent systems based on light elements have attracted particular interest [1-5]. A low density of finished products is especially valued in such areas of production as the automotive, mechanical engineering and aerospace industries [6-10]. Among all the alloys of light elements, aluminum alloys have the greatest popularity and production volume. Depending on the content of the system's main components, these alloys are divided into deformable and non-deformable, thermally hardened and non-hardened. A special group of alloys with aluminum are the Al-Si and Al-Fe subsystems. It is worth noting that iron and silicon are practically non-removable impurities, and their content is usually strictly regulated [11-13]. But the special significance of these impurities is the ability to form ternary intermetallic compounds with aluminum. The type, the quantity, the morphology and the composition of intermetallic compounds have a decisive effect on the level of mechanical properties of alloys. As production volumes increase, aluminum alloys are increasingly recycled and therefore enriched with elements such as iron, silicon, and others at each recycling stage [14-22].

The aluminum angle of the Al-Fe-Si system is characterized by the formation of an FCC solid solution, α, β, θ, τ2 (γ), τ4 (δ) and τ8 phases. In this case, the α phase usually has the morphology of Chinese writing, or a block form, has a hexagonal type of crystal lattice, and can be mainly present at high temperatures. The β phase is monoclinic, it contains less iron and more silicon and aluminum compared to the α phase. It is a low-temperature modification of the high-temperature α phase. The features of the α↔β transformation are affected by the cooling rate, ultrasonic treatment, and various additives of transition and rare earth metals. The morphology of the β phase is needle-shaped, lamellar, and can also be presented as stars. Thus, it is possible to completely suppress the α↔β transition with the formation of the αc phase with a cubic crystal lattice by introducing into the system manganese in the ratio Fe/Mn=0.5, chromium or a complex introduction of Mn and Cr, which summarizes the effect [23-28]. In commercial alloys, precipitation of intermetallic compounds is controlled by heat treatment; annealing with slow cooling and precipitation of intermetallic compounds from a supersaturated solid solution is used to separate intermetallic particles. Conversely, the quenching operation " freezes" the supersaturated solid solution. After such treatment, there are no intermetallic compounds in the metal structure; with accelerated cooling, dispersoids are formed providing the effect of thermal strengthening.

In alloys with an increased silicon and iron content, the microstructure with a continuous series of intermetallics, or a duplex microstructure, is formed. In this case, the amount of intermetallics is such that there is insufficient solid solution for their dissolution. So, their phase formation during heat treatment will differ from the generally accepted one.

This paper studies the effect of heat treatment on the microstructure of an intermetallic alloy, which mainly consists of intermetallics, in the Al-Fe-Si system.

MATERIAL AND METHODS

The study used an Al60Fe30Si10-based alloy synthesized by the additive method using horizontal consumable electrode surfacing. Commercial materials simulating the use of recycled alloys and/or scrap metal have been selected as the initial raw material for the alloy. The synthesis was performed using an electric power source for melting the alloy components, a VDM-1202 welding rectifier with an RB-301 ballast rheostat. A stationary SS-1200/SP welder's filter and ventilation table was used for the experiments. The initial components have been melted by exciting electric arc with the welding current of 290 A. Commercial aluminium alloy grade AD31N in 2 mm thick sheets, commercial steel grade St3 in 2 mm and 5 mm thick sheets, and silicon of a -500 μm fraction have been used to obtain the specified composition. A 2 mm thick steel sheet has been cut into 15 x 20 x 2 mm blanks and used as electrodes. Sheet aluminum has been cut into 100 x 30 x 2 mm blanks. Silicon has been applied to aluminum plates at the rate of 2.5 g silicon per 15 g (1 plate) of aluminum with the wet method followed by drying at room temperature within at least 12 hours.

To obtain the Al60Fe30Si10 composition, a package consisted of 4 aluminum plates with silicon deposited on them and placed on a steel base plate that was 5 mm thick. Synthesizing has been carried out under the AN-348 flux. After removing the slag crust, an alloy ingot was obtained that was cut using a Unitom-2 cutting machine with cooling into templates to determine the chemical composition and to perform metallographic analysis. The chemical composition of the synthesized alloy has been controlled using an Olympus Vanta Element-S X-ray fluorescence analyzer with the light element detection option. After determining the actual composition using ThermoCalc software version 2024a, TCAL8: Al-Allous v8.2 database, the diagram of changing the volumetric composition of the phases has been plotted. The diagram allows a better interpretation of the results and the heat treatment temperature selection. When plotting, the composition has been specified in weight %, considering the actual composition of the obtained material. Heat treatment has been carried out in a Nabertherm furnace with heating to 600 °C, holding at this temperature within 30 minutes and cooling in two modes: in water and air. After cooling, the microanalysis was carried out on an optical microscope, and the EDS analysis of phase components was performed on a scanning electron microscope. Microsections for metallographic analysis have been prepared according to the standard method on a Labotom-5 grinding machine using lubricants.

RESULTS AND DISCUSSION

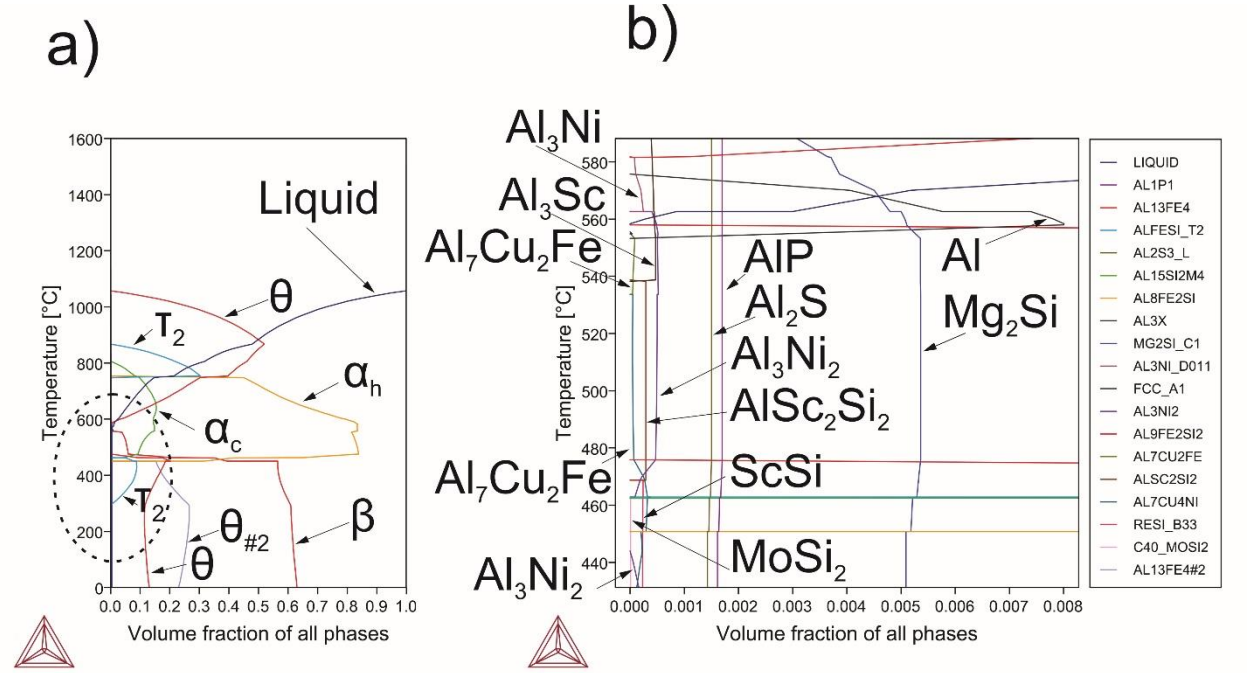

Fig. 1 Volume fraction of the all phases (a); magnified (b)

Material

This work has studied an Al-Fe-Si system alloy that is rich in both iron and silicon. It was obtained by surfacing synthesis from commercial materials and subjected to heat treatment. The initial components were steel grade 3, deformable aluminum alloy AD31N, silicon powder, and fused flux AN-348. The composition of the obtained alloy is shown in **Table 1**. The proportions of the initial components were selected based on the Al60Fe30Si10 ratio.

Table 1 Chemical composition of the synthesized material

Chemical composition, wt. %								
Al	**Fe**	**Si**	**Mn**	**Mg**	**Cr**	**Ni**	**Cu**	**Other**
60.15	30.79	7.61	1.08	0.18	0.04	0.016	0.0245	0.06

Thermodynamic calculations using the CALPHAD method

In order to bring the simulation results closer to the real situation, the actual values of the chemical composition of the alloy have been used for simulation. Based on the obtained alloy composition, the thermodynamic calculations have been performed that show the actual phase composition of the alloy at the room temperature, phase transformation temperatures and the liquidus temperature. **Fig. 1** shows the volume fraction of phases formed in the alloy under consideration in the temperature range from 1600 °C to room temperature. It can be seen that phase θ is the primary phase, which will be in the liquid, constantly interacting with it until complete crystallization at 563 °C. The cubic phase αc formed due to the presence of manganese, is released at the temperature of 807 °C. The hexagonal phase αh is formed only at the temperature of 753 °C. The transformation α↔β begins at the temperature of 558 °C and continues until the complete exhaustion of the αh phase at the temperature of 450 °C. The phase αc is present in the system up to 463 °C.

According to Sheil, the simulation assumes cooling is slow and phase formation occurs in equilibrium. The volume of the formed phases shows that aluminides and silicides with impurity elements are most actively formed at the temperature of ~600 °C in the amount proportional to the impurity content in the alloy. In this case, aluminum compounds with phosphorus and sulfur precipitate at 1136 °C and 863 °C, respectively. At room temperature, the θ phase is present in two modifications. At room temperature, the entire volume of the alloy consists of intermetallics: 63 % β and 36.5 % θ. The remaining 0.5 % are silicides and aluminides. Thus, it has been revealed that secondary materials, such as commercial aluminum alloys and steel, can be used to obtain Al-Fe-Si system alloys. This approach allows significant reducing the cost of the resulting alloys. Based on the simulation results, it has been decided to select the heat treatment temperature of 600 °C.

Alloy "as prepared"

As a result of additive synthesis, an alloy that almost entirely consisted of β and θ intermetallic phases has been obtained. The results of thermodynamic modeling are in good agreement with the microanalysis data. However, the solid solution of aluminum located in the intermetallic space can be seen in the microstructural photographs, **Fig. 2**. The β and θ phases have been formed simultaneously, which agrees with the data on the temperatures of phase transformations obtained during modeling. The areas between the intermetallic particles are practically free of impurity atoms, where the solid solution of aluminum crystallizes. The discrepancy between the phase composition data at room temperature in the "as prepared" state is due to crystallization under non-equilibrium conditions. Most aluminides and silicides are concentrated in the area free of β/θ intermetallic phases. At the same time, the intermetallic particles are not represented by stars, needles, or plates, as is typical for most system alloys under consideration, which have a lower content of silicon and iron.

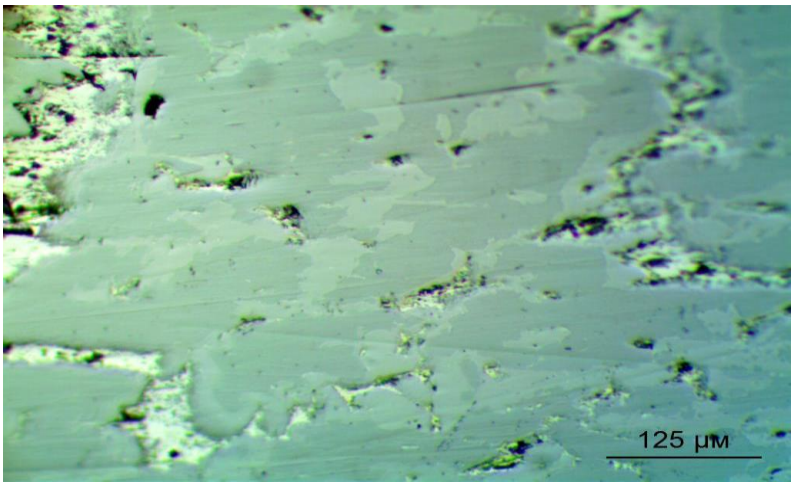

Fig. 2 Optical image of the alloy microstructure in the "as prepared" state

Microstructure evolution in the heat treatment

Fig. 3 shows the microstructure after heat treatment. The cooling rate does not fundamentally affect the morphology of the alloy's intermetallic components, but it does lead to certain changes in their composition.

To understand better the phase transformations that occur in the alloy upon cooling from 600 °C, it is necessary to refer to its phase diagram. During holding at the heat treatment temperature, complete dissolution in the aluminum solid solution will not occur due to the composition. At this temperature, the phase transition of 85 % of the alloy composition to the hexagonal phase αh and 12 % to the cubic phase αc formed due to the presence of manganese will be observed. An insignificant number of liquid accounts for the remaining ~3 %, i.e. melting can be observed in certain areas of the sample, as well as a residual amount of the high-temperature phase θ. Upon cooling in the temperature range of 558-463 °C, the phase transition α↔β will occur, and the final phase composition will differ slightly from the composition corresponding to the phase diagram due to the non-equilibrium cooling conditions. Taking into account the accelerated (compared to equilibrium) cooling, the complete transformation α↔β does not occur, and in this case, the low-temperature phase θ is formed first, the crystals of which serve as nuclei for the formation of the remaining phases. With cooling in water, in addition to the θ phase, the θ#2 phase is formed. It differs in that the aluminum atoms are partially replaced by silicon atoms. The EDS analysis records the θ#2 phase with the composition of Al (60.9-62.43) Fe (35.12-35.71)Si(2.45-3.38) wt%. Silicon is in the phase at the solubility level in the aluminum solid solution. Based on the θ phase particles, precipitates of the α phase with the composition of Al (56.95-60.38) Fe (35.07-35.60)Si(6.92-7.45) wt% are also detected. Such enrichment of the θ phase with silicon coincides with the results obtained in [30]. Partial replacement of aluminum atoms by silicon atoms in the θ phase provides prerequisites for the formation of FCC aluminum regions, including those with dissolved silicon atoms in the amount of up to 4 %. The growth of intermetallic phases occurs before the collision of particles or before the critical depletion of the region around the growing particle in silicon and iron atoms. At room temperature, the depleted region is represented by an FCC solid solution of aluminu

a)

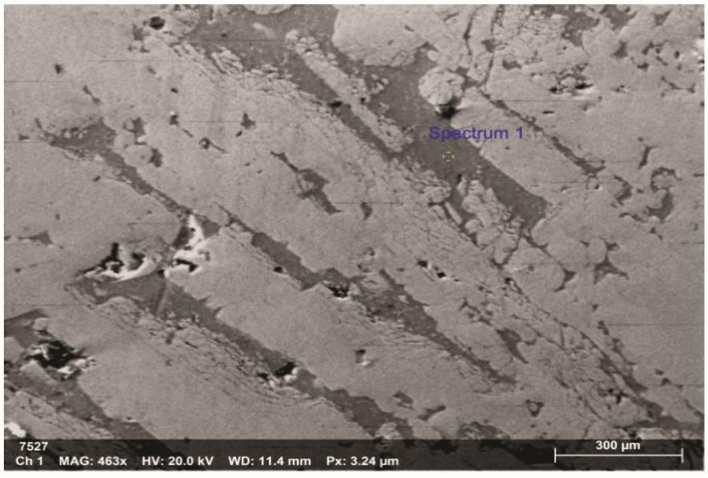

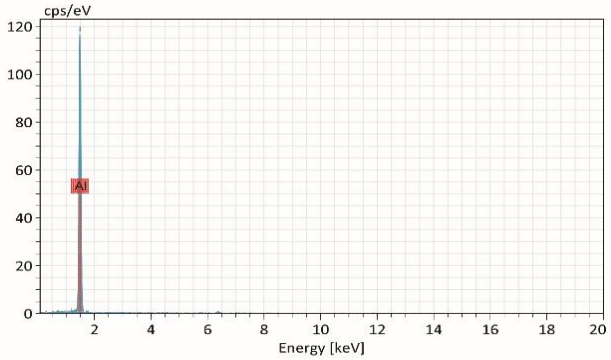

Fig. 3 a SEM image of the alloy microstructure and spectrum for the FCC region of aluminum after heat treatment at 600 °C with cooling in water (a)

b)

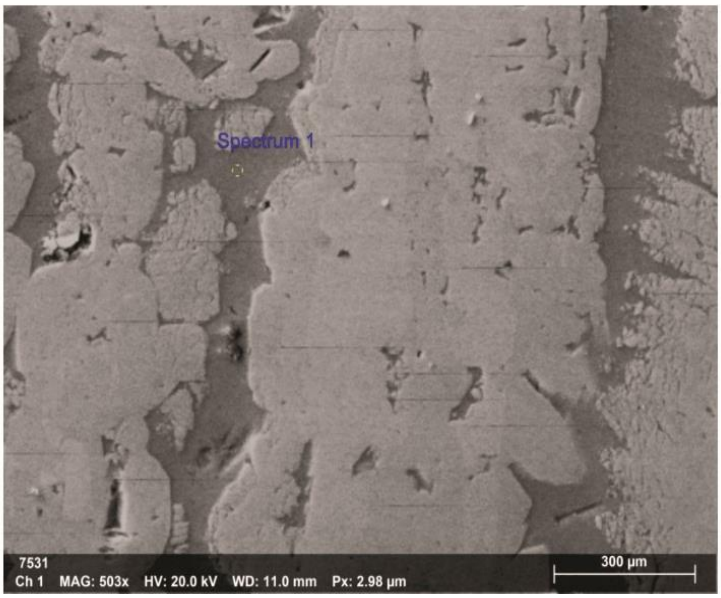

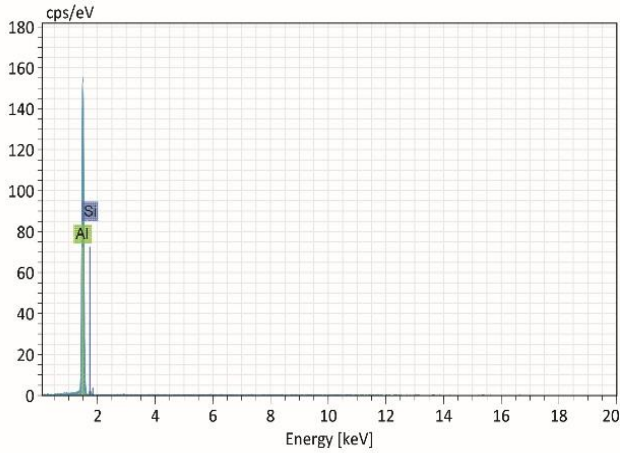

Fig. 3 b SEM image of the alloy microstructure at 600 °C - in air (b)

With decreasing the cooling rate, a slight increase in the size of intermetallic particles is observed. In this case, the FCC regions have sizes of 50-150 µm by 1000-1500 µm for water and air cooling. With cooling in air, the θ#2 phase with dissolved silicon is also observed in the structure, but the amount of the θ phase with the composition of Al (62.47-62.91) Fe (37.09-37.53) predominates. In addition, a transition phase θ' with the composition of Al (88.88-90.23) Fe (9.77-11.12) has been detected.

CONCLUSION

The study has studied the phase formation of a multicomponent alloy based on the Al-Fe-Si system obtained using commercial alloys by the additive method and reached the following conclusions.

1. When using commercial alloys as initial components, impurities present in the alloys can act as alloying elements and form insoluble impurities/inclusions. Thus, the presence of such harmful impurities as sulfur and phosphorus leads to the formation of silicides and aluminides that are not removed into the slag. Impurities of molybdenum, magnesium, nickel and scandium dissolve poorly in the alloy, forming insoluble compounds. Copper is also prone to the formation of individual phases. The total amount of silicides and nitrides formed corresponds to the amount of the elements that create them in the initial alloys.
2. Thermodynamic modeling allows successful prediction of the phase composition of the alloy, considering all the impurities present; in general, the impurities present in the original alloys do not significantly affect the phase composition of the alloys compared to using only pure components.
3. Manganese can be reduced from slag, penetrating the metal and transforming the hexagonal αh phase into the cubic αc phase.
4. As a result of heat treatment at the maximum content of the α phase, the transformation β↔α occurs during heating and holding, the nature of the transformation α↔β is determined by the cooling conditions.
5. During accelerated cooling in water, the monoclinic phase θ is enriched with silicon atoms, a certain amount of the α phase is observed framing the intermetallic particles θ, and during slow cooling in air, the transition phase θ' with an increased aluminum content is formed.

Acknowledgements: This research was funded by the Science Committee of the Ministry of Science and Higher Education of the Republic of Kazakhstan (Grant No. AP19675471).

REFERENCES

1. K. S. Tun, P. Murugan, T. S. Srivatsan, M. Gupta: Materials Today: Proceedings, 46, 2021, 1210-1214. https://doi.org/10.1016/j.matpr.2021.02.066.
2. I. Chang, Q. Cai: Progress in Materials Science, 123, 2022, 100779. https://doi.org/10.1016/j.pmatsci.2021.100779.
3. Y. N. Mansurov, A. R. Rikhsiboev, S. Y. Mansurov: Metallurgist, 63, 2020, 1303–1312. https://doi.org/10.1007/s11015-020-00952-7.
4. M. Zhang, Y. Tian, X. Zheng, Y. Zhang, L. Chen, J. Wang: Materials, 16(3), 2023, 1065. https://doi.org/10.3390/ma16031065.
5. J. Wen, J. Cheng, X. Min, Y.vHuang, Y.bLiu: Journal of Alloys and Compounds, 1002, 2024, 175537. https://doi.org/10.1016/j.jallcom.2024.175537.
6. F. Czerwinski: Materials, 13(15), 2020, 3441. https://doi.org/10.3390/ma13153441.
7. T. A. Baser, E. Umay, V. Akıncı: The Eurasia Proceedings of Science Technology Engineering and Mathematics, 21, 2022, 79-87. https://doi.org/10.55549/epstem.1227541.
8. A. K. Sharma, R. Bhandari, A. Aherwar, R. Rimašauskienė, C. Pinca-Bretotean: Materials Today: Proceedings, 26, 2020, 2419-2424. https://doi.org/10.1016/j.matpr.2020.02.516.
9. Q. Zhang, Y. Zhu, X. Gao, Y. Wu, C. Hutchinson: Nature Communications, 11, 2020, 5198. https://doi.org/10.1038/s41467-020-19071-7.
10. R. Chandel, N. Sharma, S. A. Bansal: Emergent Materials, 4, 2021, 1243–1257. https://doi.org/10.1007/s42247-021-00186-6.
11. S. Miladinović, B. Stojanović, S. Gajević, A. Vencl: Silicon, 15(6), 2023, 2507-2527. https://doi.org/10.1007/s12633-022-02216-2.
12. M. H. Khan, A. Das, Z. Li, H. R. Kotadia: Intermetallics, 132, 2021, 107132. https://doi.org/10.1016/j.intermet.2021.107132.

13. C. Choudhary, H. N. Bar, S. M. Arif, K. L. Sahoo, D. Mandal: Journal of Materials Engineering and Performance, 33(10), 2024, 5155-5167. https://doi.org/10.1007/s11665-023-08313-6.
14. Z. Que, C. Fang, C. L. Mendis, Y. Wang, Z. Fan: Journal of Alloys and Compounds, 932, 2023, 167587. https://doi.org/10.1016/j.jallcom.2022.167587
15. V. Andreyachshenko, I. Bartenev, Y. Malashkevichute-Brillant: Acta Metallurgica Slovaca, 30(3), 2024, 133-136. https://doi.org/10.36547/ams.30.3.2065.
16. A. Z. Aiken, V. A. Andreyachshenko: AIP Conference Proceedings, 3251(1), 2024, 040006. https://doi.org/10.1063/5.0234067.
17. V. A. Andreyachshenko, M. K. Ibatov: AIP Conference Proceedings, 3251(1), 2024, 040001. https://doi.org/10.1063/5.0234066.
18. V. A. Andreyachshenko, M. K. Ibatov: Metallurgical Research & Technology, 121(3), 2024, 315. https://doi.org/10.1051/metal/2024035.
19. V.A. Andreyachshenko: Kovove materialy-Metallic materials, 60(2), 2022, 79-87. https://doi.org/10.31577/km.2022.2.79.
20. V. A. Andreyachshenko, Y. Isheva, A. Mazhit, D. Imangazinova: Materiali in Tehnologije, 53(6), 2019, 805-810. https://doi.org/10.17222/mit.2018.250.
21. A. B. Naizabekov, V. A. Andreyachshenko: Metallurgist, 57 (1-2), 2013, 159–163. https://doi.org/10.1007/s11015-013-9706-0.
22. V. Andreyachshenko: Materials Letters, 254, 2019, 433–435. https://doi.org/10.1016/j.matlet.2019.07.127.
23. D. Zhang, X. Wang, Li, H. Zhang, H. Nagaumi: Intermetallics, 131, 2021, 107103. https://doi.org/10.1016/j.intermet.2021.107103.
24. P. Orozco-González, M. Castro-Román, R. Muñiz-Valdez, S. Luna-Álvarez, F. Equihua-Guillén, A. Hernández-Rodríguez, V. H. Baltazar-Hernández, F. Alvarado-Hernández: Materials Letters, 180, 2016, 277-279. https://doi.org/10.1016/j.matlet.2016.05.139.
25. H. Jiang, Y.C. Liu, C. Wei, Y. H. Zhang, Z. M. Gao: Journal of Alloys and Compounds, 466(1–2), 2008, 92-97. https://doi.org/10.1016/j.jallcom.2007.11.019.
26. J. M. Yu, N. Wanderka, A. Rack, R. Daudin, E. Boller, H. Markötter, A. Manzoni, F. Vogel, T. Arlt, I. Manke, J. Banhart: Journal of Alloys and Compounds, 766, 2018, 818-827. https://doi.org/10.1016/j.jallcom.2018.06.372.
27. D. Song, Y. Jia, Q. Li, Y. Zhao, W. Zhang: Materials, 15(4), 2022, 1618. https://doi.org/10.3390/ma15041618.
28. E. de Rosso, C. A. dos Santos, A. Garcia: Advanced Engineering Materials, 24(8), 2022, 2001552. https://doi.org/10.1002/adem.202001552.